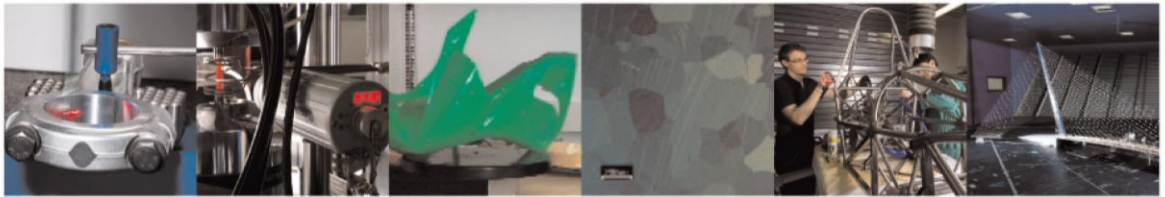




**POLITECNICO**  
MILANO 1863

DIPARTIMENTO DI MECCANICA



## Processability of pure Cu by LPBF using a ns-pulsed green fiber laser

Singh A.; Caprio L.; Previtali B.; Demir A.G.

This is a post-peer-review, pre-copyedit version of an article published in OPTICS AND LASER TECHNOLOGY. The final authenticated version is available online at:

<http://dx.doi.org/10.1016/j.optlastec.2022.108310>

This content is provided under [CC BY-NC-ND 4.0](https://creativecommons.org/licenses/by-nc-nd/4.0/) license



# Processability of pure Cu by LPBF using a ns-pulsed green fiber laser

Ashutosh Singh, Leonardo Caprio, Barbara Previtali, Ali Gökhan Demir\*

Department of Mechanical Engineering, Politecnico di Milano, Via La Masa 1, 20156 Milan, Italy

\*Corresponding author: [aligokhan.demir@polimi.it](mailto:aligokhan.demir@polimi.it)

## Abstract

Visible wavelength lasers appear a straightforward solution for improved density in LPBF of Cu. However, only few high power continuous wave (CW) green lasers are industrially available. Nanosecond (ns) pulsed green laser sources can be appealing for a wider industrial use, if adapted towards a melting-based process avoiding ablation based shockwaves. This work reports the use of a novel ns-pulsed green fiber laser with 100 W average power and 30 MHz pulse repetition rate for processing pure Cu. The work shows that free-standing samples without excessive powder ejection from the powder bed and densities of 98.1% can be achieved with processing conditions similar to a conventional CW lasers.

Keywords: pure copper; green laser; pulsed wave

## 1 Introduction

Laser powder bed fusion (LPBF) with Cu can boost the efficiency of heat transfer devices thanks to the possibility of producing complex geometries [1]. While low absorption of copper towards the commonly used near infrared (NIR) fiber laser source [2–5] in LPBF makes the full melting of metallic powder difficult, its high thermal conductivity tends to destabilize the melt pool. Different strategies have been used to tackle the processability of pure Cu such as using high power NIR continuous wave (CW) lasers [2,3], multiple pass strategies [4], small beam sizes accompanied by fine powders [6], improved optical absorptivity via powder modifications [7,8] and high temperature preheating [9]. The use of visible wavelength lasers is a more recent development. The use of blue diode lasers has been limited to large beam sizes [10,11]. The use of green lasers on the other hand is limited to especially availability. Conventionally a green laser is a solid state laser (eg. Nd:YAG, fiber or disc operating at 1030–1080 nm) with the second harmonic generation (530–540 nm). Few examples show their use in LPBF [12–14]. While improved processability of Cu with visible wavelength lasers is an established fact, the research concerning the different type of laser architectures is still an open field.

High power CW green lasers are difficult to manufacture and maintain stable. The harmonic crystals used in the generation of the green wavelength are sensitive to the heat induced with the high power CW laser emission. While the lifetime of a NIR fiber laser is associated to the lifetime of the pumping diodes, for a green fiber laser it is associated to the much shorter lifetime of the harmonic generator. The use of a harmonic generator with ns-long pulsed wave (PW) systems is an established method. Commonly such lasers have been employed for processing Cu alloys, glass, and ceramics in ablation-based micromachining applications [15–17]. The ns-pulsed lasers are generally characterized by high peak powers ( $P_{pk} > 10$  kW) and are not suited for LPBF as they induce severe powder ejection and powder bed instability due to the shockwave generated during ablation [18]. Such laser sources have been used in the early

LPBF research [19] and successively abandoned as the CW fiber lasers became commercially available. Today commercial LPBF systems operate with NIR fiber lasers run at CW or power modulated PW mode with  $\mu\text{s}$ -long pulses [20]. With these lasers the light-material interaction is melting dominated and the LPBF process follows a well-known trend in densification as function of the energy density starting from low-energy density caused lack-of-fusion, moving towards a stable plateau of high density, and with excessive energy density generating keyhole porosity [21]. Recently, novel ns-pulsed laser sources with high average ( $P > 50 \text{ W}$ ), low peak power ( $P_{\text{pk}} < 5 \text{ kW}$ ) and very high pulse repetition rates (PRR at MHz level) have been made available, which can provide a Quasi-CW (QCW) emission profile [22]. Stable green lasers can be made with such emission profiles, which can be exploited in LPBF coming close to a CW process due to the elevated pulsation frequency even though duty cycles levels are below 10%.

This work studies the LPBF feasibility of pure Cu using a new generation of ns-pulsed green fiber laser with 30 MHz pulse repetition rate and 100 W average power. The paper shows the system configuration and studies the processability through a large experimental campaign assessing the effect of the main process parameters on the apparent density.

## 2 Experimental systems

### 2.1 Materials

This work was carried out using gas atomized pure copper powder (Cu 99.9% wt, O 0.08% wt, P < 0.15% wt) (LPW Technology Ltd, Runcorn, UK). The powder particle size was  $+15 \mu\text{m}/-45 \mu\text{m}$ . Base plate materials was AISI 316L stainless steel (Cr 16-18 wt%, Ni 10-14 wt%, Mo 2-3 wt%, Mn 2 wt%; C < 0.03 wt%, Fe bal). A SEM image of the powder is shown in Figure 1.a.

### 2.2 Laser powder bed fusion (LPBF) system

The LPBF of copper powder was carried out with a flexible prototype system named *Powderful* (Figure 1.b). The system was equipped with a ns-pulsed single-mode pulsed fiber laser (GLPN-100-M, IPG Photonics, Cambridge, USA) with a central emission wavelength of 532 nm. The laser is based on a MOPA (master oscillator power amplifier) active fiber laser architecture. The seed laser is emitted at NIR, sent to a remote amplifier, where it is amplified to the power level and converted to the green wavelength. The laser was characterized by  $P = 100 \text{ W}$  average power, emitting  $\tau = 1.4 \text{ ns}$  pulses with a fixed pulse repetition rate at  $\text{PRR} = 30 \text{ MHz}$ . The maximum peak power of the pulses was calculated as  $P_{\text{pk}} = 2.4 \text{ kW}$  with a maximum pulse energy of  $E = 3 \mu\text{J}$ . The rise time of the laser source to the average emission power corresponded to  $400 \mu\text{s}$ . Its effect over the deposition process was minimized by employing serpentine scanning strategy during the tests which did not consider switching on and off of the process emission when jumping between adjacent scan tracks.

The beam was manipulated using a scanner head (Superscan II, Raylase, Wessling, Germany) coupled to focus shifting optics (Focusshifter, Raylase, Wessling, Germany) and an F-theta lens with nominal focal length of 260 mm (SL-532-165-260, Wavelength Opto-electronic, Singapore). The combined optical system yielded an effective working distance of 244 mm from the F-theta lens. In this configuration, the measured smallest spot diameter at the working plane was  $d_0 = 38 \mu\text{m}$ . The measured laser beam size in x and y axes and different positions of the focus shifting optics is reported in Figure 1.c. The caustic shape of the beam propagation at different positions of the focus shifter is shown in Figure 1.d. The figures show that the beam size is controllable on the powder bed without changing the caustic propagation significantly.

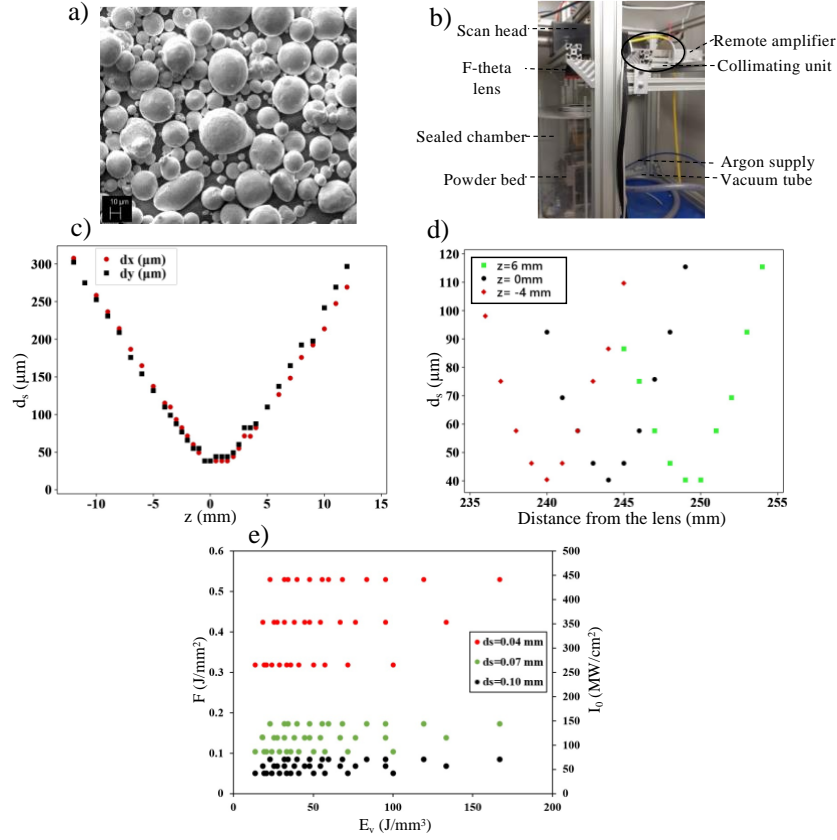


Figure 1 (a) SEM image of gas atomized pure copper powder. (b) the open LBPF platform Powderful fitted with the ns-pulsed green fiber laser, (c) spot size at the powder bed with variable lens position, (d) Spot size measured at different planes with fixed lens position. (e) The resulting energy density, peak irradiance, and peak fluence values employed in the experimental campaign.

### 3 Experimental campaign

The experimental campaign aimed to analyze the feasibility of the proposed laser source. Three levels of laser power ( $P$ ), scan speed ( $v_s$ ), hatch distance ( $h$ ), and spot size ( $d_s$ ) with two levels of layer thickness ( $z$ ) were set and specimens corresponding to all parameter combinations were produced. Specimens with a dimension of  $5 \times 5 \times 5 \text{ mm}^3$  were built directly on the substrate without any support structures in an inert atmosphere of argon on AISI 316 stainless steel substrate with  $45^\circ$  hatch rotation between the subsequent depositions employing a serpentine scanning strategy. The set of fixed and variable parameters are reported in Table 1.

Relative density ( $\rho$ ) of the produced specimens were analyzed via cross-section images by measuring the proportion of the solidified area over the total area in the image [23] using optical microscope (Mitutoyo Quick Vision ELF QV-202). Analysis of variance (ANOVA) was applied to the results analyzing the parameter interactions up to the second order. Statistical significance level was set at  $\alpha=5\%$ . The results were also analyzed as a function of energy density ( $E_v$ ) expressed by:

$$E_v = \frac{P}{v_s \cdot h \cdot z} \quad (1)$$

The mapping of the power and energy densities in the different conditions tested are reported graphically in Figure 1.e where peak irradiance ( $I_0$ ) and peak fluence ( $F$ ) of a single pulse were calculated according to the following formulas [24]:

$$I_0 = \frac{8P_{pk}}{\pi d_s^2} \quad (2)$$

$$F = \frac{8E}{\pi d_s^2} \quad (3)$$

Table 1 Fixed and variable parameters for the LPBF process

Fixed parameter	Value
Inert Gas	Argon
Substrate Material	AISI 316 Stainless Steel
Hatch Rotation Angle	45°
Variable Factor	Level
Average power, P (W)	60; 80; 100
Scan speed, $v_s$ (mm/s)	300; 600; 900
Hatch distance, h (mm)	0.04; 0.07; 0.1
Layer thickness, z (mm)	0.05; 0.07
Spot size, $d_s$ (mm)	0.04; 0.07; 0.10

#### 4 Results and discussions

Figure 2 shows representative images of the powder bed taken through the protective window after the recoating and during the scanning of a layer. It can be seen that the powder bed remains within and between the layers. In particular, in the investigated conditions there are not regions where powder is missing due to a violent ejection caused by the ablation shockwave.

Figure 3.a shows examples of free-standing Cu samples built at 60 W of power. Majority of the samples showed no evidence of macro defects. Specimens produced with  $z=70 \mu\text{m}$ ,  $P=60 \text{ W}$ , and  $v_s=900 \text{ mm/s}$  were delaminated, due to the low energy density. Figure 3.b. shows a subset of the experimental plan with the cross-section images. It can be seen that the process shows mainly lack-of-fusion pores with the porosity decreasing towards higher power and slower scan speed. Figure 3.c and d show the main effects and interaction plots of the process parameters. Table 2 shows the ANOVA results, which confirm the statistical significance of all the process parameters and the interactions between  $P*v_s$ ,  $P*h$ , and  $v_s*d_s$ . It can be seen that  $P$ ,  $v_s$ ,  $h$ , and  $z$  show the expected trends from an LPBF process, increasing the density as the energy density is increased.

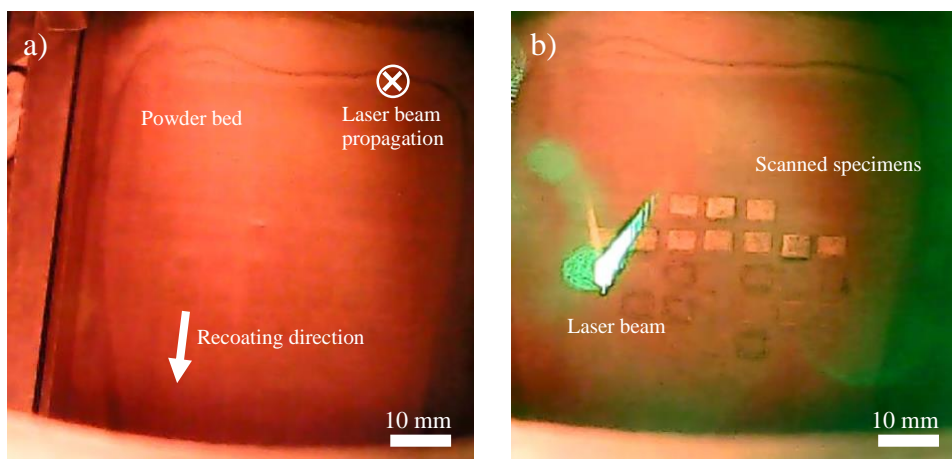


Figure 2 Powder bed images acquired with an external camera through the protective window of the LPBF system. (a) Powder bed after the recoating of a new layer. (b) Powder bed during the scanning of the laser beam.

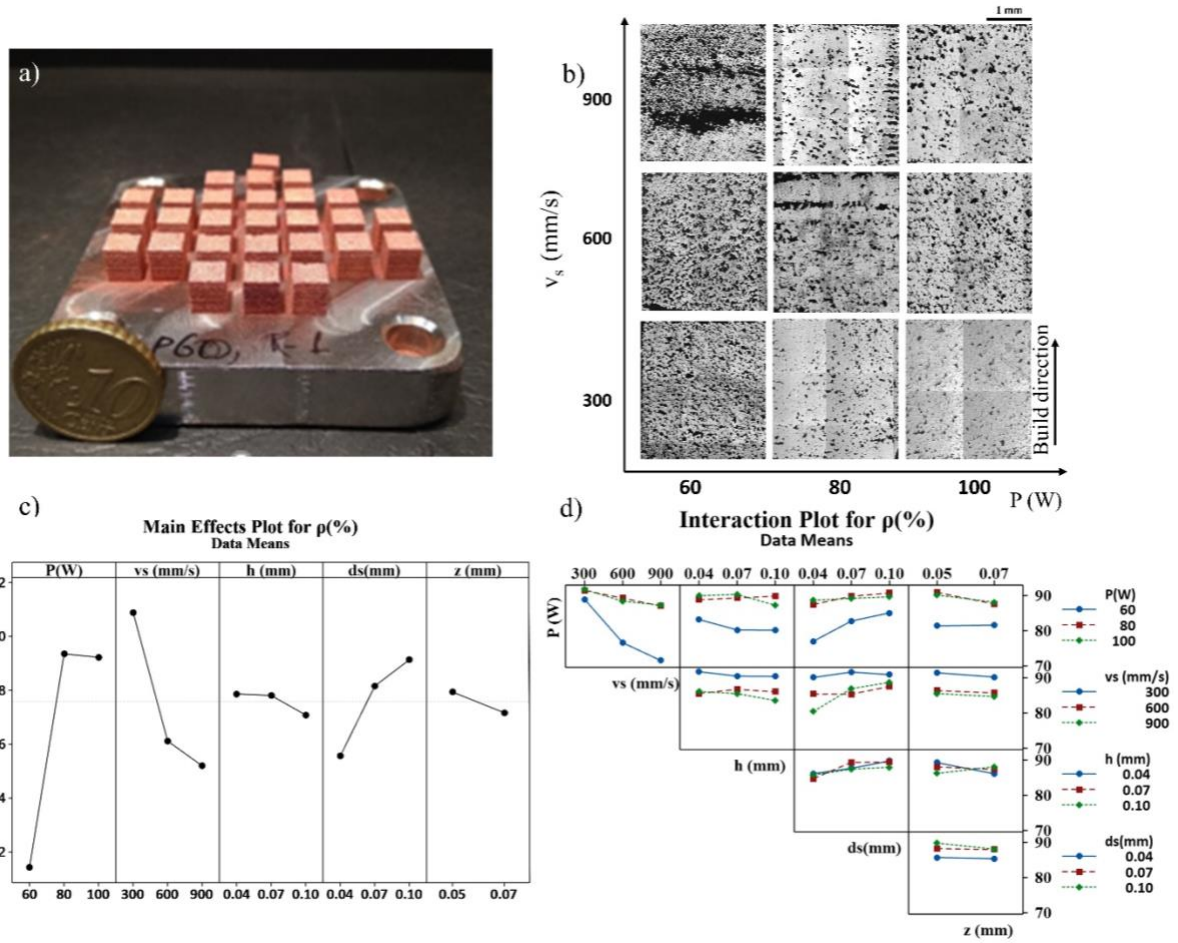


Figure 3 (a) Macro images of the specimens produced during the experimental runs at  $P=60$  W and  $z=0.05$  mm. (b) Influence of scan speed and power on the specimen density with  $z=0.05$  mm;  $d_s=0.04$  mm and  $h=0.04$  mm. (c) Main effect plot for  $p$ (%). (d) Interaction plot for  $p$ (%).

A peculiar behaviour is observed with  $d_s$ , where larger beams appear to improve the density. The cross-section images of the specimens produced with  $z=50$   $\mu$ m,  $h=0.1$  mm,  $P=80$  W,  $v_s=300$  mm/s and with different  $d_s$  is reported in Figure 4. As confirmed by the ANOVA analysis, larger process diameters are beneficial to the densification process. This can be attributed to the fact that very small beams may generate conditions close to ablation which may induce powder ejection from the bed [18][25]. This type of severe powder bed denudation through powder ejection at higher levels of peak irradiance was qualitatively observed in terms of the powder flying from the powder bed and depositing in the chamber. In the examined regime, the issue related to the peak irradiance regards the powder ejection rather than keyholing and keyhole porosity. The results showed that for a stable process the peak irradiance with the medium or the largest beam size can be potentially used, which is up to approximately 144 MW/cm<sup>2</sup>.

Melt ejections and powder denudation have been observed in detail via X-ray transmissive imaging by Hojjatzadeh *et al.* during pulsed wave LPBF due to the sudden peak power emission over the melt[26]. This is coherent with the model of the keyhole formation process by Semak *et al.*, where vapour ejections due Knudsen layer formation at elevated peak temperatures will generate disturbances in the neighbourhood of the melt[27]. The mitigating impact of reducing the peak emission power via beam defocusing will impact the localised vapour generation and thus the Knudsen flow which has been reported to be a significantly influencing factor over powder denudation by Matthews *et al.*[28]. In terms of short to ultrashort pulsed lasers, the single laser pulse ablates the material, generating a plasma with a



relatively short life time. The measurements in literature show that the following shockwave generation and the plume expansion may last in the order of a few microseconds [29]. Employing multiple pulses the plume generation was found to be further increased [30,31]. Such ejection mechanisms can be expected to be locally more violent compared to the vapour pressure achieved in LPBF with CW lasers generating localized powder bed denudation.

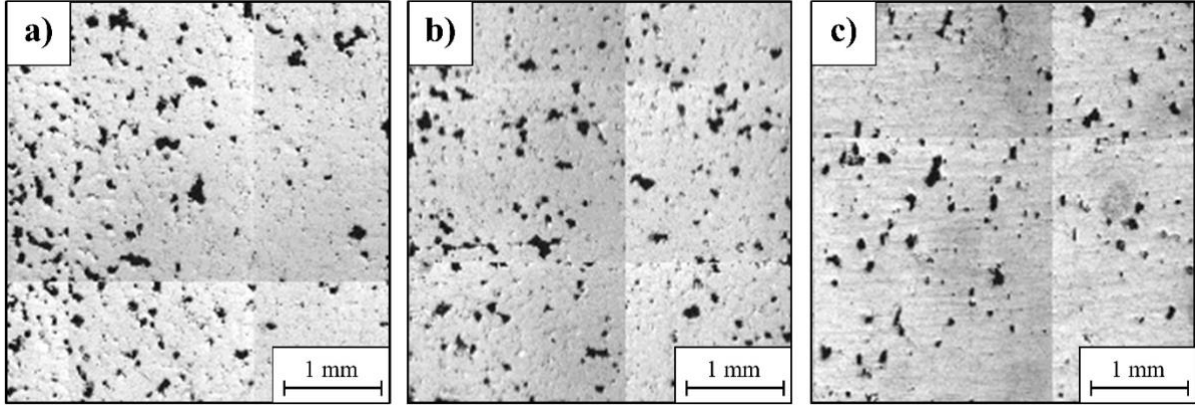


Figure 4 Cross-section of the specimens produced at same process parameters with  $E_v = 54 \text{ J/mm}^3$  but at different  $d_s$  and consequently  $I_0$  (a)  $d_s = 0.04 \text{ mm}$ ,  $I_0 = 354 \text{ MW/cm}^2$ ,  $\rho = 93 \%$  (b)  $d_s = 0.07 \text{ mm}$ ,  $I_0 = 115 \text{ MW/cm}^2$ ,  $\rho = 94 \%$  (c)  $d_s = 0.1 \text{ mm}$ ,  $I_0 = 57 \text{ MW/cm}^2$ ,  $\rho = 96 \%$

Figure 5.a shows the relative density as a function of the energy density grouped by different spot sizes. A large variation in terms of density can be observed, that is typical of pure Cu processing. On the other hand, the processed energy density levels ( $20\text{--}180 \text{ J/mm}^3$ ) are much smaller than what is reported in literature using CW NIR lasers ( $200\text{--}2000 \text{ J/mm}^3$ ) [32]. Evidently the higher optical absorption of the green wavelength improved the process efficiency. Presumably, the high thermal conductivity remains the issue resulting in the high variability. As shown in Figure 5.b, density levels at 98.1% can be readily achieved.

The results overall show that the high PRR and relatively low  $P_{pk}$  of the ns-pulsed laser source provides an effective solution for improved density in LPBF of pure Cu. The duty cycle ( $\delta$ ) can be used to compare the emission profiles between different PW laser technologies:

$$\delta = \tau \cdot PRR \quad (4)$$

The duty cycle used in this work is much lower than those used with  $\mu\text{s}$  pulsed power modulated fiber lasers ( $\delta > 90\%$ ) [20]. Compared to a typical ns-pulsed NIR laser used for ablation (eg.  $P = 50 \text{ W}$ ,  $PRR = 50 \text{ kHz}$ ,  $\tau = 100 \text{ ns}$ ,  $\delta = 0.5\%$ ,  $P_{pk} = 10 \text{ kW}$ ), the employed green laser provides higher duty cycle ( $\delta = 4\%$ ) and lower peak power ( $P_{pk} \leq 2.4 \text{ kW}$ ). Metelkova et al employed a similar 30 ns-pulsed laser operating at 1070 nm wavelength during the LPBF of maraging steel for the purpose of powder removal on the built surfaces to expose them for successive surface polishing by a CW laser [18]. With  $1.4 \text{ GW/cm}^2$  peak irradiance ( $P = 42 \text{ W}$ ,  $PRR = 100 \text{ kHz}$ ,  $\tau = 30 \text{ ns}$ ,  $\delta = 0.3\%$ ,  $P_{pk} = 14 \text{ kW}$ ) the generated shockwaves were able to remove powder up to 4 mm in depth after 20 consecutive scans. The use of femtosecond pulsed laser sources has also been shown in literature, producing much lower density values [25]. Indeed, a typical fs-pulsed laser used for ablation (eg.  $P = 10 \text{ W}$ ,  $PRR = 10 \text{ MHz}$ ,  $\tau = 150 \text{ fs}$ ,  $\delta = 0.00015\%$ ,  $P_{pk} = 7 \text{ MW}$ ) can be expected to denude the powder bed but also provide an indirect melting process through the heating provided by the intense plasma on the laser-material interaction zone. In the light of the powder bed stability observations and the density results, it can be concluded that the emission profile of the employed laser source is suitable for a melting-based

process similar to a CW laser. The results still require further improvement in terms of density and therefore the thermal, electrical, and mechanical properties.

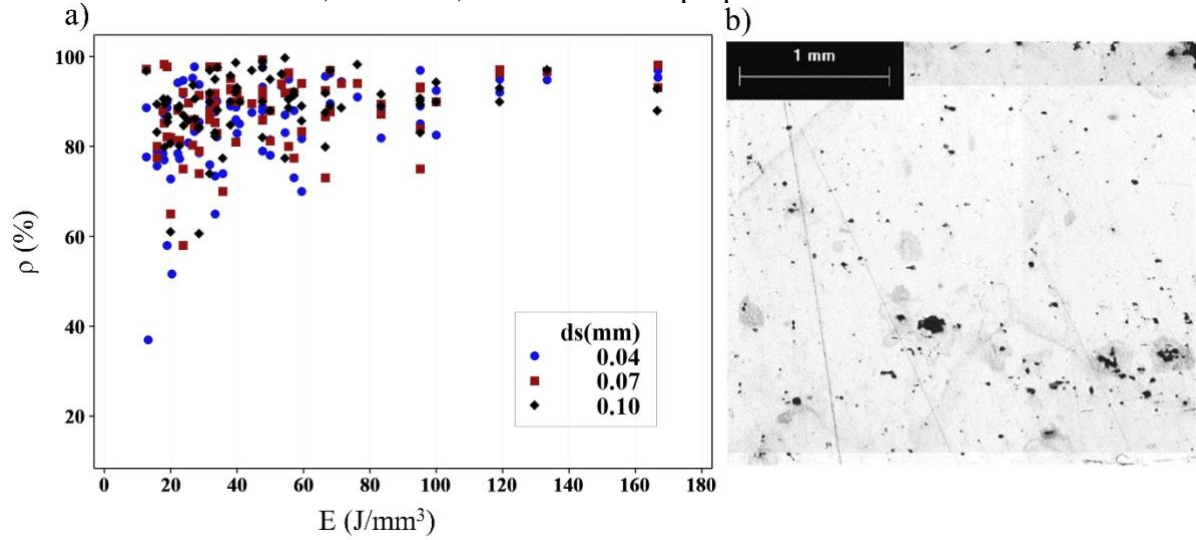


Figure 5 (a) Apparent density as a function of the energy density and spot size. (b) Cross-section of the specimen produced with  $P=100\text{W}$ ,  $v_s=300\text{mm/s}$ ,  $h=0.04\text{mm}$ ,  $d_s=0.07\text{mm}$ ,  $z=0.05\text{mm}$ ,  $E=166\text{ J/mm}^3$ ,  $I_0=144\text{ MW/cm}^2$ ,  $\rho=98.1\%$ .

Table 2 Analysis of variance table for  $\rho$  (%). Statistically significant parameters are shown in *italic*.

Source	DF	Adj SS	Adj MS	F-Value	P-Value
P(W)	2	3775.8	1887.90	43.92	<i>0.000</i>
$v_s$ (mm/s)	2	3287.2	1643.60	38.23	<i>0.000</i>
h (mm)	2	330.0	165.02	3.84	<i>0.023</i>
$d_s$ (mm)	2	562.4	281.20	6.54	<i>0.002</i>
z (mm)	1	478.6	478.65	11.13	<i>0.001</i>
P(W)* $v_s$ (mm/s)	4	1858.3	464.57	10.81	<i>0.000</i>
P(W)*h (mm)	4	468.4	117.10	2.72	<i>0.030</i>
P(W)* $d_s$ (mm)	4	252.3	63.07	1.47	0.213
P(W)*z (mm)	2	45.7	22.85	0.53	0.588
$v_s$ (mm/s)*h (mm)	4	130.3	32.58	0.76	0.554
$v_s$ (mm/s)* $d_s$ (mm)	4	481.9	120.49	2.80	<i>0.027</i>
$v_s$ (mm/s)*z (mm)	2	138.8	69.41	1.61	0.201
h (mm)* $d_s$ (mm)	4	24.2	6.06	0.14	0.967
h (mm)*z (mm)	2	162.8	81.39	1.89	0.153
$d_s$ (mm)*z (mm)	2	66.0	33.01	0.77	0.465
Error	228	9801.7	42.99		
Lack-of-Fit	104	4895.8	47.08	1.19	0.176
Pure Error	124	4905.8	39.56		
Total	269	19017.1			

## 5 Conclusion

This work showed the use of a novel green fiber laser based on high pulse repetition rate and low peak power suited to a melting based light/material interaction. The green laser showed improved process efficiency producing relatively high density specimens (>98%) with lower energy density levels compared to NIR sources. The work showed that the process follows a similar densification behaviour compared to conventional LPBF systems operating with CW and long PW lasers. Larger beam diameters were effective in improving the density of the samples and this could be correlated to a mitigation of the powder ejection phenomena at lower levels of irradiance. However, porosity issues related to lack-of-fusion could still be identified. The presented results show progress at a preliminary development phase of the system and demonstrate the applicability of such laser technology for consolidation of the copper powder bed. Additional studies will involve the use of advanced scanning strategies, high preheating



solutions or different powder size distributions for improving the part density. From this perspective, the relatively more consolidated architecture of the ns-pulsed laser source may help a greater diffusion of green wavelength lasers in the industry by reducing the capital and the maintenance costs.

## Acknowledgements

The Italian Ministry of Education, University and Research is acknowledged for the support provided through the Project "Department of Excellence LIS4.0 - Lightweight and Smart Structures for Industry 4.0". The authors are grateful to IPG Photonics for the longstanding collaboration and Raylase for the technical support.

## References

- [1] Wong M, Tsopanos S, Sutcliffe CJ, Owen I. Selective laser melting of heat transfer devices. *Rapid Prototyp J* 2007;13:291–7. doi:10.1108/13552540710824797.
- [2] Ikeshoji TT, Nakamura K, Yonehara M, Imai K, Kyogoku H. Selective Laser Melting of Pure Copper. *Jom* 2018;70:396–400. doi:10.1007/s11837-017-2695-x.
- [3] Colopi M, Caprio L, Demir AG, Previtali B. Selective laser melting of pure Cu with a 1 kW single mode fiber laser. *Procedia CIRP* 2018;74:59–63. doi:10.1016/J.PROCIR.2018.08.030.
- [4] Colopi M, Demir AG, Caprio L, Previtali B. Limits and solutions in processing pure Cu via selective laser melting using a high-power single-mode fiber laser. *Int J Adv Manuf Technol* 2019;104. doi:10.1007/s00170-019-04015-3.
- [5] WilliamM. Steen · JyotirmoyMazumder. *LaserMaterial Processing* 4th Edition. n.d. doi:10.1007/978-1-84996-062-5.
- [6] Sinico M, Cogo G, Benettoni M, Calliari I, Pepato A. Influence of powder particle size distribution on the printability of pure copper for selective laser melting. *Solid Free Fabr 2019 Proc 30th Annu Int Solid Free Fabr Symp - An Addit Manuf Conf SFF* 2019 2019;657–66.
- [7] Jadhav SD, Vleugels J, Kruth JP, Van Humbeeck J, Vanmeensel K. Mechanical and electrical properties of selective laser-melted parts produced from surface-oxidized copper powder. *Mater Des Process Commun* 2020;2:1–8. doi:10.1002/mdp2.94.
- [8] Jadhav SD, Dadbakhsh S, Vleugels J, Hofkens J, Puyvelde P Van, Yang S, et al. Influence of carbon nanoparticle addition (and impurities) on selective laser melting of pure copper. *Materials (Basel)* 2019;12. doi:10.3390/ma12152469.
- [9] Malý M, Koutný D, Pantělejev L, Pambaguian L, Paloušek D. Effect of high-temperature preheating on pure copper thick-walled samples processed by laser powder bed fusion. *J Manuf Process* 2022;73:924–38. doi:10.1016/j.jmapro.2021.11.035.
- [10] Asano K, Tsukamoto M, Funada Y, Sakon Y, Abe N, Sato Y, et al. Copper film formation on metal surfaces with 100 W blue direct diode laser system. *J Laser Appl* 2018;30:032602. doi:10.2351/1.5040635.
- [11] Hori E, Sato Y, Shibata T, Tojo K, Tsukamoto M. Development of SLM process using 200 W blue diode laser for pure copper additive manufacturing of high density structure. *J Laser Appl* 2021;33:012008. doi:10.2351/7.0000311.
- [12] Trumpf. World premiere at Formnext: green laser from TRUMPF prints copper and gold 2018. [https://www.trumpf.com/it\\_IT/impresa/stampa/comunicatistampa/comunicato-stampa-pagina-con-i-dettagli/release/world-premiere-at-formnext-green-laser-from-trumpf-](https://www.trumpf.com/it_IT/impresa/stampa/comunicatistampa/comunicato-stampa-pagina-con-i-dettagli/release/world-premiere-at-formnext-green-laser-from-trumpf-)

- prints-copper-and-gold/.
- [13] Nordet G, Gorny C, Mayi Y, Daligault J, Dal M, Efferneilli A, et al. Absorptivity measurements during laser powder bed fusion of pure copper with a 1 kW cw green laser. *Opt Laser Technol* 2022;147:107612. doi:10.1016/j.optlastec.2021.107612.
  - [14] Gruber S, Stepien L, López E, Brueckner F, Leyens C. Physical and geometrical properties of additively manufactured pure copper samples using a green laser source. *Materials (Basel)* 2021;14. doi:10.3390/ma14133642.
  - [15] Jackson MJ, O'Neill W. Laser micro-drilling of tool steel using Nd:YAG lasers. *J Mater Process Technol* 2003;142:517–25. doi:10.1016/S0924-0136(03)00651-4.
  - [16] Demir AG, Previtali B. Remote cutting of Li-ion battery electrodes with infrared and green ns-pulsed fibre lasers. *Int J Adv Manuf Technol* 2014;75:1557–68. doi:10.1007/s00170-014-6231-7.
  - [17] Jiang S, Wang Q, Jiang L, Zhu X. Frequency-doubled short nanosecond fiber lasers for glass drilling and grinding. *Int J Appl Ceram Technol* 2022;3–8. doi:10.1111/ijac.13994.
  - [18] Metelkova J, Ordnung D, Kinds Y, Van Hooreweder B. Novel strategy for quality improvement of up-facing inclined surfaces of LPBF parts by combining laser-induced shock waves and in situ laser remelting. *J Mater Process Technol* 2021;290:116981. doi:10.1016/j.jmatprotec.2020.116981.
  - [19] Morgan R, Sutcliffe CJ, O'Neill W. Density analysis of direct metal laser re-melted 316L stainless steel cubic primitives. *J Mater Sci* 2004;39:1195–205. doi:10.1023/B:JMSC.0000013875.62536.fa.
  - [20] Demir AG, Colombo P, Previtali B. From pulsed to continuous wave emission in SLM with contemporary fiber laser sources: effect of temporal and spatial pulse overlap in part quality. *Int J Adv Manuf Technol* 2017;91:2701–14. doi:10.1007/s00170-016-9948-7.
  - [21] Cacace S, Semeraro Q. About Fluence and Process Parameters on Maraging Steel Processed by Selective Laser Melting: Do They Convey the Same Information? *Int J Precis Eng Manuf* 2018;19:1873–84. doi:10.1007/s12541-018-0204-y.
  - [22] Gapontsev V, Avdokhin A, Kadwani P, Samartsev I, Platonov N, Yagodka R. SM green fiber laser operating in CW and QCW regimes and producing over 550W of average output power. *Nonlinear Freq Gener Convers Mater Devices, Appl XIII, Proc SPIE* 2014;8964:896407. doi:10.1117/12.2058733.
  - [23] Spierings AB, Schneider M, Eggenberger R. Comparison of density measurement techniques for additive manufactured metallic parts. *Rapid Prototyp J* 2011;17:380–6. doi:10.1108/13552541111156504.
  - [24] Demir AG, Pangovski K, O'Neill W, Previtali B. Investigation of pulse shape characteristics on the laser ablation dynamics of TiN coatings in the ns regime. *J Phys D Appl Phys* 2015;48:235202. doi:10.1088/0022-3727/48/23/235202.
  - [25] Kaden L, Matthäus G, Ullsperger T, Engelhardt H, Rettenmayr M, Tünnermann A, et al. Selective laser melting of copper using ultrashort laser pulses. *Appl Phys A Mater Sci Process* 2017;123:1–6. doi:10.1007/s00339-017-1189-6.
  - [26] Hojjatzadeh SMH, Guo Q, Parab ND, Qu M, Escano LI, Fezzaa K, et al. In-situ characterization of pore formation dynamics in pulsed wave laser powder bed fusion. *Materials (Basel)* 2021;14:1–11. doi:10.3390/ma14112936.
  - [27] Semak V V, Hopkins JA, Mccay MH, Mccay TD. A concept for a hydrodynamic model of keyhole formation and support during laser welding. *Int. Congr. Appl. Lasers Electro-Optics*, vol. 1994, 1994, p. 641–50. doi:10.2351/1.5058848.
  - [28] Matthews MJ, Guss G, Khairallah SA, Rubenchik AM, Depond PJ, King WE. Denudation of metal powder layers in laser powder bed fusion processes. *Acta Mater*

- 2016;114:33–42. doi:10.1016/j.actamat.2016.05.017.
- [29] Demir AG, Pangovski K, O'Neill W, Previtali B. Investigation of pulse shape characteristics on the laser ablation dynamics of TiN coatings in the ns regime. *J Phys D Appl Phys* 2015;48. doi:10.1088/0022-3727/48/23/235202.
  - [30] Pangovski K, Sparkes M, Cockburn A, Neill WO, Teh PS, Lin D, et al. Control of Material Transport Through Pulse Shape Manipulation — A Development Toward Designer Pulses. *IEEE J Sel Top Quantum Electron* 2014;20.
  - [31] Pangovski K, O'Neill W, Teh PS, Alam S, Richardson D, Demir AG. Designer Pulses for precise machining of silicon - A step towards photonic compositions. *ICALEO 2012 - 31st Int. Congr. Appl. Lasers Electro-Optics*, 2012, p. 999–1008.
  - [32] Horn TJ, Gamzina D. Additive Manufacturing of Copper and Copper Alloys. *ASM Handbook, Vol 24, Addit. Manuf. Process.*, vol. 24, ASM International; 2020, p. 388–418. doi:10.31399/asm.hb.v24.a0006579.